Preprint
UCRL-JC-147456

Crystallization of Beryllium-Boron Metallic Glasses

A. F. Jankowski, M. A. Wall, T. G. Nieh

This article was submitted to
131st Annual Meeting and Exhibition of the Minerals, Metals and Materials Society, Seattle, WA., February 17-21, 2002

February 14, 2002

U.S. Department of Energy

Lawrence
Livermore
National
Laboratory

This work was performed under the auspices of the United States Department of Energy by the University of California, Lawrence Livermore National Laboratory under contract No. W-7405-Eng-48.

CRYSTALLIZATION OF BERYLLIUM-BORON METALLIC GLASSES

A.F. Jankowski, M.A. Wall, and T.G. Nieh

Lawrence Livermore National Laboratory, 7000 East Avenue, Livermore, CA 94550

ABSTRACT

Prior studies of evaporation and sputter deposition show that the grain size of pure beryllium can be dramatically refined through the incorporation of metal impurities. Recently, the addition of boron at a concentration greater than 11% is shown to serve as a glassy phase former in sputter deposited beryllium. Presently, thermally induced crystallization of the beryllium-boron metallic glass is reported. The samples are characterized during an in-situ anneal treatment with bright field imaging and electron diffraction using transmission electron microscopy. A nanocrystalline structure evolves from the annealed amorphous phase and the crystallization temperature is affected by the boron concentration.

INTRODUCTION

Beryllium (Be) metal and its alloys are of major importance in the space and nuclear industries.[1-2] It has a low density, high elastic modulus, elevated melting point, high heat capacity, and good nuclear hardness. These attributes make Be attractive for space structures and optical mirrors.[3-4] For example, when used for space mirror sensors, Be is ideal because its low density and high micro-yield strength.[5] The high micro-yield strength, i.e. stress that gives rise to a 10^{-6} plastic strain, is required to remain undistorted during fast space maneuvers. However, Be also suffers from some intrinsic problems such as low ductility and poor manufacturability that limit it from wider use. It's generally accepted that the low ductility is associated with its hexagonal close packed (hcp) structure, localized slip, and high impurity

content (especially that of BeO in Be powder products). Efforts have been made but with little success to improve ductility either by alloying to change the crystal structure from hcp to body centered cubic (bcc) or by forming intermetallic beryllides. [6-7] Although some binary and ternary phase diagrams were developed as a result of these efforts, general information on the phase relationship between Be and other elements is extremely limited.

In another application, a promising target design for plasma physics studies of inertial confinement fusion is a uniformly thick and atomically smooth Be capsule. [8] The performance advantages for Be of lower opacity, a larger ablation rate, more initial mass, and higher bulk strength than polymeric counterparts are accompanied by demanding material requirements. Since Be capsules are usually produced by coating a thin-wall polymer mandrel using a sputter deposition process, the corresponding textured and crystalline growth of Be produces an intrinsic roughness in the capsule surface even when using in-situ smoothing processes as ion bombardment. [9-12] A possible alternative to using crystalline Be for producing an atomically smooth surface and a homogeneous microstructure could be a Be-rich metallic glass. [11-12]

In general, the material properties of vapor deposited coatings are sensitive to the growth morphology and microstructure of the deposit. For example, the variation of sputter deposition parameters as working gas pressure and flow along with substrate temperature and applied bias are known to affect the formation of crystalline phases in BN films. [13-15] Of particular interest with regards to creating smooth Be coatings is the sputter deposition of pure boron (B) as an amorphous coating. [13] Since B has a similar density to molecular weight ratio as Be, it's feasible to use B as a substitutive element for Be in coatings for ICF targets. [10-12] In fact, it's demonstrated through co-sputter deposition that the alloying of B with Be leads to glassy phase formation in thick coatings. [16] The Be-B binary phase diagram [17] has a eutectic at 11 at.% B, beyond which the amorphous $Be_{1-x}B_x$ phase is found. Often deep eutectics indicate that a structure of a liquid, i.e. an amorphous phase, can be stabilized at low temperature. The rapid quench that's needed to stabilize a glassy solid phase from the melt or gaseous phase is accomplished through sputter deposition process. [18] In this study, the thermal stability of a

nanocrystalline (x = 0.10) and amorphous $Be_{1-x}B_x$ (x = 0.16 and 0.21) coatings are examined to provide insight to the nature of the amorphous to crystalline transition.

EXPERIMENTALS

The $Be_{1-x}B_x$ coatings are synthesized by sputter deposition onto substrates of polished silicon using planar magnetrons. The deposition chamber contains a circular array of three planar magnetron sources. The sputter deposition targets are fully dense, powder compacts. A detailed patented procedure [19] for preparation of a pure and fully dense, boron target is described elsewhere. The pure Be target (chemically assayed at 99.4 at.% purity) and a $Be_{.90}B_{.10}$ alloy target are produced by the hot-isostatic pressing of powder precursors in vacuum-sealed tantalum containers. The magnetron sources are operated in the dc mode with discharge voltages of 360 V and 520 V for the Be and B targets, respectively. The deposition chamber is cryogenically pumped to a base pressure of 5×10^{-6} Pa. An argon sputter gas pressure 0.25-0.4 Pa is maintained using a using a flow rate of 25-35 cm^3 min^{-1}. Nominal deposition rates from the B and Be targets are 0.07 and 0.16 nm $(W\ min)^{-1}$, respectively. The substrates are located 6 cm beneath the center of the sputter source array. The nominal composition of the $Be_{1-x}Be_x$ alloy coating is computed from calibrated deposition rates, as confirmed through measurements using contact profilometry and an electron microprobe.

The 0.4-3 μm thick coatings are prepared for bright field imaging in plan view with a transmission electron microscope (TEM). The sample preparation for plan view imaging involves thinning the reverse side of the substrate through mechanical polishing followed by ion milling at glancing incidence. The preparation for imaging in cross-section involves epoxying two wafer pieces face-to-face and then encapsulating in a metal tube from which 0.2-0.4 mm thick disks are cut. [20] The 3 mm diameters disks are then lapped to a thickness less than 0.1 mm, dimpled, and ion milled in a liquid nitrogen cold stage. The bright field and diffraction pattern imaging is conducted using a JEOL 200CX electron microscope. Bright field imaging reveals the presence or lack of a microcrystalline structure and

the selected-area diffraction patterns (SADPs) are used to determine the crystalline phase. To assess the stability of the as-deposited structure, the samples are vacuum annealed in-situ during TEM imaging. The temperature of the specimen holder is initially heated to 200 °C. The sample is then heated to 500 °C in 25 °C increments with a 20 min. hold time at each temperature. The accuracy of measuring the sample temperature is ±10 °C based on calibrations on known phase transformations.

RESULTS & ANALYSIS

The as-deposited $Be_{1-x}B_x$ coatings are nanocrystalline with a host hcp Be lattice [11-12] up to a concentration of 11 at.% B and then amorphous [16] above that eutectic composition. To examine the stability of the amorphous phase, two of the amorphous as-deposited coatings are examined in cross-section using the TEM while being annealed in-situ. The bright field images for the 16 at.% B and 21 at.% B coatings are shown (Figs. 1a-n) with a progression in temperature. As the temperature is elevated to and held at just 200 °C (Fig. 1b), the onset of crystallization is observed in the 16 at.% B coating. Nanocrystallites appear as small regions of diffraction contrast that are less than 5 nm in size. The number and size of these regions increase as the temperature is further raised in sequence to 250 °C (Fig. 1c), 275 °C (Fig. 1d), 300 °C (Fig. 1e), 325 °C (Fig. 1f) and 350 °C (Fig. 1g). For the 21 at.% B coating, there is no evidence of crystallization in the bright images (Figs. 1h-k) through an anneal temperature of 275 °C. At 300 °C (Fig. 1l), some diffraction contrast becomes evident, similar to that observed for the 16 at.% B sample at 200 °C (Fig. 1b). At 325 °C, the diffracting regions (Fig. 1m) are 20 nm in size, about the same in size although much fewer in number than for the 16 at.% B sample. At 350 °C, the 16 at.% B and 21 at.% B samples have similar microstructures (Figs. 1g and 1n, respectively).

SADPs are taken to assess phase formation associated with the crystallization of the amorphous $Be_{1-x}B_x$ coatings. For example, the SADPs are shown for the 21 at.% B sample in the as-deposited condition (Fig. 2a) and as annealed at 350 °C (Fig. 2b). Both patterns are taken using an exposure time of 2 min. (Usable SADPs were not generated at the lower temperature anneals due to instrument

limitations.) The as-deposited phase has no crystalline reflections (Fig. 2a). Only a diffuse halo associated with the amorphous phase is seen as centered at a spacing equivalent to 0.164 nm. At 350 °C, the reflections are well defined in the SADP (of Fig. 2b) with measured interplanar (d) spacings listed in Table 1. The d-spacings and indexed reflections are listed in Table 1 for comparison to the established phases of hcp Be and cubic Be_2B that are found in the Be-rich end of the Be-B phase diagram as well as for hcp BeO that may form during the in-situ anneal as a consequence of surface oxidation. Note that there are no matches in any of the $Be_{1-x}B_x$ coatings ($x < 1$) to the primary reflections of (101), (102), (200), (104), and (211) for the tetragonal $Be_{5-n}B_n$ phase(s) (n is an integer) where the corresponding d-spacings are .303 nm, .243 nm, .168 nm, .156 nm, and .147 nm, respectively. The crystallized 21 at.% B sample has an hcp Be phase as indicated by the characteristic [21] d-spacings for the (10.0), (00.2) and (10.1) reflections measured as 0.196 nm, 0.178 nm and 0.173 nm, respectively. In addition, the formation of Be_2B is evident in the characteristic d-spacings for the (111), (220) and (311) reflections of 0.267 nm, 0.163 nm and 0.140 nm, respectively. Although it's unnecessary to include a BeO phase identification for this sample, it does appear in the as-deposited nanocrystalline samples with less than 11 at.% B. [16]

The evolution of microstructure and phase changes in the as-deposited, crystalline $Be_{1-x}B_x$ coatings can be useful for interpretation of the crystallization mechanism in the amorphous phase. A sample with 10 at.% B is annealed, in-situ to 500 °C. The microstructure of the as-deposited coating is imaged in plan view (Fig. 3a) with its corresponding SADP (Fig. 3b) and at 500 °C (Fig. 3c) with its corresponding SADP (Fig. 3d). The microstructure shows little (if any) observable change with in-situ annealing at 500 °C from the as-deposited structure [16] that has a 15 nm grain size. The diffraction patterns change with anneal temperature. The d-spacings for the 10 at.% B sample are listed in Table 1 in the as-deposited (25 °C) condition and as taken at the anneal temperatures of 300 °C, 400 °C and 500 °C, respectively. In the as-deposited condition, the host phase of the 10 at.% B sample is hcp Be as indicated by the characteristic reflections of (10.0), (00.2) and (10.1) with measured d-spacings of 0.199 nm, 0.181 nm and 0.174 nm, respectively. Unlike the amorphous $Be_{1-x}B_x$ samples, there is some evidence of a native hcp BeO phase present with the as-deposited crystalline condition even though this sample has a high concentration of 10 at.% B. As the specimen is heated to 300 °C, the appearance of the (220)

reflection characteristic of cubic Be_2B is found with a measured d-spacing of 0.165 nm. At 400 °C and 500 °C, the additional cubic Be_2B reflections of (111) and (311) are found with corresponding d-spacings of 0.267 nm and 0.140 nm, respectively.

The crystalline deposit of 10 at.% B can be considered a supersaturated solid solution of hcp Be. Diffusion in the solid state and consequent phase separation into Be_2B occurs for a low temperature, in-situ anneal of only 300 °C. Yet microstructural imaging reveals no coarsening of the nanocrystalline, as-deposited structure. The amorphous $Be_{1-x}B_x$ samples are metastable with crystallization temperature dependence on the B concentration. The 16 at.% B sample evidences localized nucleation of nanocrystals at only 200 °C, with subsequent progressive coarsening and increased number of nucleation sites as temperature is increased to 350 °C. The 21 at.% B sample evidences localized nanocrystallization at a higher temperature of 300 °C. However, the nucleation rate and coarsening is much faster for the 21 at.% B sample than in the 16 at.% B sample, as by 350 °C both microstructures for the 16 at.% B and 21 at.% B samples are essentially equivalent. At 350 °C, the crystalline structures show evidence of phase separation into cubic Be_2B and hcp Be. The temperature dependent evolution of nucleation sites for crystallization and the increasing size of the nanocrystals in the 16 at.% B sample suggests a diffusion regulated process as does the appearance of phase separation in the SADPs. The supersaturation of the 21 at.% B sample appears more stable, compared to the 16 at.% B sample, with a higher temperature for the onset of crystallization from the amorphous as-deposited structure. To evolve the same microstructure as the 16 at.% B sample at 350 °C, the kinetics of diffusion are faster for the 21 at.% B sample. The increased d-spacings for the as-deposited nanocrystalline $Be_{1-x}B_x$ samples indicates expansion of the host hcp Be lattice. Upon annealing, as well as phase separation, the expansion of the hcp Be lattice is relaxed as seen in the d-spacing measurements for the 10 at.% B sample as well as that for the crystallized 21 at.% B sample.

DISCUSSION

It's widely known from studies of evaporation and sputter deposition that the grain size of nominally pure (99.8 at.%) Be can be dramatically refined through the incorporation of metallic impurities [22] as well as refractory metals [23-26] at greater concentrations. In this study, the stability of an amorphous $Be_{1-x}B_x$ phase is evaluated for B concentrations greater than 11 at.% B. In addition to observing a B concentration-temperature dependent crystallization of the amorphous phase, the onset of phase separation to Be_2B is observed as well from a supersaturated solid solution of crystalline hcp $Be_{0.90}B_{0.10}$. Thus, it may be unlikely that polymorphous crystallization occurs for amorphous $Be_{1-x}B_x$ in which there is no change of composition. It appears the kinetics of the transition to the crystalline phase from the amorphous involves a diffusion-controlled phenomenon, i.e. the amorphous phase may undergo some short range ordering prior to crystallization. This may be inferred from dispersed nucleation sites and the growth of the crystalline phase in the amorphous matrix. It doesn't appear certain that the crystallization mechanism first involves separation of the homogeneous, as-deposited glassy phase into distinct glassy phases. Nor would it seem likely the mechanism is that of primary crystallization in which the first crystals to form have a composition different from the glass since a supersaturated solid solution of B in Be is demonstrated in the as-deposited nanocrystalline structures for concentrations up to 11 at.% B. Perhaps a eutectic crystallization mechanism (or a variant thereof) may occur in which the glass transforms to the two crystalline phases growing in closely coupled from. After all, the average spacing associated with the amorphous halo is that of the (220) reflection for Be_2B. The presence of a $Be_{5-n}B_n$ phase, in either the as-deposited or annealed coatings, is unlikely since there are no unique d-spacings for this phase measured in diffraction. Although there is no overall composition change between the glass and the eutectic colony, the rate of growth is likely controlled by some solute (B) diffusion just ahead of the amorphous-crystalline interface. Hence, crystallization of the amorphous phase with greater B concentration may have a larger barrier to initiate but then proceeds with faster kinetics. The crystallization of the $Be_{1-x}B_x$ phase may be similar, for example, to that [27] observed for the Fe-Ni-P-B system.

The transition of the amorphous $Be_{1-x}B_x$ ($x > 0.11$) phase into a nanocrystalline phase is not an unexpected phenomena. The use of 5-13 % metalloids to prepare metallic glasses for transition into

microcrystalline alloys with grain sizes under a micron is demonstrated for the synthesis of materials with useful high-temperature properties as stabilized by finely dispersed borides. [28-29] In future work, the concentration dependent crystallization of the $Be_{1-x}B_x$ phase with phase separation will be assessed using differential scanning calorimetry. From the present work, the lower temperatures observed for the crystallization (which are greater than the glass transition temperature) of the sputter deposited coatings with respect to the melting point would seem to indicate that the stabilization of the amorphous phase in the bulk may be difficult. The sputter deposition process produces very fast quench rates from the vapor to the solid phase that can easily be several orders of magnitude greater than for bulk processes. Specifically, the reduced glass transition temperature [30-31] is less than 0.4 for the 21 at.% B sample (noting the crystallization temperature is less than 600 K and its corresponding melt point of about 1500K) whereas ratios of about 0.50 to 0.66 or larger are often associated with bulk glass formation.

SUMMARY

The thermal stability of sputter-deposited, amorphous $Be_{1-x}B_x$ coatings for concentrations greater than 11 at.% B is examined using TEM with in-situ anneal treatments. Bright field imaging of the microstructure and selected area diffraction of the interplanar spacings for phase identification are used to characterize the coatings in plan view and cross section. It appears that a concentration dependent temperature for crystallization is observed in amorphous $Be_{1-x}B_x$. Evidence of crystallization is seen at 200 °C for a 16 at.% B coating whereas an anneal temperature greater than 300 °C is required for crystallization of a 21 at.% B sample. The observation of phase separation in the crystallized phase may possibly suggest a mechanism of eutectic crystallization.

ACKNOWLEDGMENTS

The authors thank Phil Ramsey for his contributions to the synthesis of the coatings. This work was performed under the auspices of the U.S. Department of Energy by University of California, Lawrence Livermore National Laboratory under contract No. W-7405-Eng-48.

REFERENCES

1. D. Webster and G.J. London, Beryllium Science and Technology, Vol. 1, (Plenum Press, New York and London, 1979).

2. D.R. Floyd and J.N. Lowe, Beryllium Science and Technology, Vol. 2, (Plenum Press, New York and London, 1979).

3. R.J. Switz, in Beryllium Science and Technology, Vol. 2, pp. 231-247, edited by D.R. Floyd and J.N. Lowe, (Plenum Press, New York and London, 1979).

4. L.A. Grant, in Beryllium Science and Technology, Vol. 2, pp. 249-273, edited by D.R. Floyd and J.N. Lowe, (Plenum Press, New York and London, 1979).

5. T.G. Nieh and J. Wadsworth, Scripta. Mater. **38**, p. 863 (1998).

6. A. Aldinger and G. Petzow, in Beryllium Science and Technology, Vol. 1, pp. 235-305, edited by D. Webster and G.J. London, (Plenum Press, New York and London, 1979).

7. T.G. Nieh and J. Wadsworth, Scripta Metall. Mater. **24,** p. 1489 (1990).

8. S. Haan, Phys. Plasmas **2**, p. 2480 (1995).

9. C.W. Chen and C.S. Alford, J. Vac. Sci. Technol. **A6**, p. 128 (1988).

10. R. M^{c}Eachern, C. Alford, R. Cook, D. Makowiecki, and R. Wallace, Fusion Technol. **31**, p. 435 (1997).

11. A.F. Jankowski, P. Ramsey, M. M^{c}Kernan, and J.D. Morse, in Amorphous and Nanostructured Carbon, Vol. 593, pp. 489-92, eds. J. Robertson, J. Sullivan, O. Zhou, T. Allen, and B. Coll, (Mater. Res. Soc. Symp. Proc., Pittsburgh, PA, 2000).

12. A. Jankowski, in Structure and Mechanical Properties of Nanophase Materials, Vol. 634, Ch. 3, pp. 15.1-15.6, ed. D. Farkas, H. Kung, M. Mayo, H. van Swygenhoven, and J. Weertman, (Mater. Res. Soc. Symp. Proc., Pittsburgh, PA, 2001).

13. A. Jankowski, J. Hayes, M. M^{c}Kernan and D. Makowiecki, Thin Solid Films **308-9**, p. 94 (1997).

14. A. Jankowski and J.P. Hayes, Diamond Relat. Mater. 7, p. 380 (1997).

15. I. Jiménez, A. Jankowski, L. Terminello, D. Sutherland, J. Carlisle, G. Doll, W. Tong, D. Shuh, and F. Himpsel, Phys. Rev. B **55**, p. 12025 (1997).

16. A.F. Jankowski, M.A. Wall, and T.G. Nieh, "Composition Effects on the Crystallinity of Beryllium-Rich Coatings", UCRL-MI-134990-Rev1, (Lawrence Livermore National Laboratory, Livermore, CA, 2001).

17. T. Massalski, (ed.), in Binary Alloy Phase Diagrams, ASM International, Metals Park, Ohio, p. 341 (1987).

18. H. Liebermann, in Amorphous Metallic Alloys, pp. 26-41, ed. F. Luborsky, (Butterworth and Co. Publ., London, G.B., 1983).

19. D. Makowiecki and M. McKernan, "Fabrication of Boron Sputter Targets", U.S. Patent No. 5,392,981 (February 28, 1995).

20. S.B. Newcomb, C. Boothroyd, and W. Stobbs, J. Microsc. **140**, p. 195 (1985).

21. J. McKay, and M. Hill, J. Nucl. Mater. **8**, p. 263 (1963).

22. R. Adams and C. Nordin, Thin Solid Films **181**, p. 375 (1989).

23. L. Tanner, and R. Ray, Acta Metall. **27**, p. 1727 (1979).

24. L. Tanner, Scripta Metall. **145**, p. 657 (1980).

25. C. Severin, C. Chen, A. Belova, and M. Lin, J. Appl. Phys. **52**, p. 1850 (1981).

26. C. Gilbert, R. Ritchie, and W.L. Johnson, Appl. Phys. Lett. **71**, p. 476 (1997).

27. D.G. Morris, Scripta Metall. **16,** p. 585 (1982).

28. R. Ray, J. Mater. Sci. **16**, p.2924 (1981).

29. R. Ray, in Rapidly Solidified Amorphous and Crystalline Alloys, p. 435, ed. B.H. Kear, B.C. Giessen and M. Cohen, (Mater. Res. Soc. Symp. Proc., North-Holland, Amsterdam, 1982).

30. D. Turnbull and J.C. Fisher, J. Chem. Phys. **17**, p. 71 (1949).

31. D. Turnbull, J. Chem. Phys. **18**, p. 198 (1950).

TABLES

Table I. – Interplanar spacings (nm) of $Be_{1-x}B_x$ coatings

hcp Be		hcp $Be_{.50}O_{.50}$		cubic $Be_{.67}B_{.33}$		$Be_{.90}B_{.10}$				$Be_{.79}B_{.21}$	
(hk.l)	d(nm)	(hk.l)	d(nm)	(hkl)	d(nm)	25°C	300°C	400°C	500°C	25°C	350°C
				(111)	.2690			.2666	.2666		.2667
		(10.0)	.2337	(200)	.2335	.2354	.2222	.2313	.2292		.2307
		(00.2)	.2188								
		(10.1)	.2062								
(10.0)	.1980					.1990	.1899	.1965	.1959		.1961
(00.2)	.1793					.1808		.1793	.1778		.1781
(10.1)	.1733					.1738	.1718	.1723	.1737		.1722
				(220)	.1648		.1646	.1637	.1627	(.164)	.1632
		(10.2)	.1598						.1504		
				(311)	.1407				.1387		.1400
		(11.0)	.1349	(222)	.1347	.1363					.1330
(10.2)	.1329					.1334		.1324	.1314		
		(10.3)	.1238				.1277				
		(20.0)	.1168	(400)	.1166						.1156
(11.0)	.1143	(11.2)	.1149			.1145		.1136	.1149		.1131
		(20.1)	.1129						.1129		
		(00.4)	.1095				.1091				
				(331)	.1070						.1062
(10.3)	.1023	(20.2)	.1031	(420)	.1043	.1023		.1019	.1015		.1012
(20.0)	.0989	(10.4)	.0991				.0979	.0986	.0981		

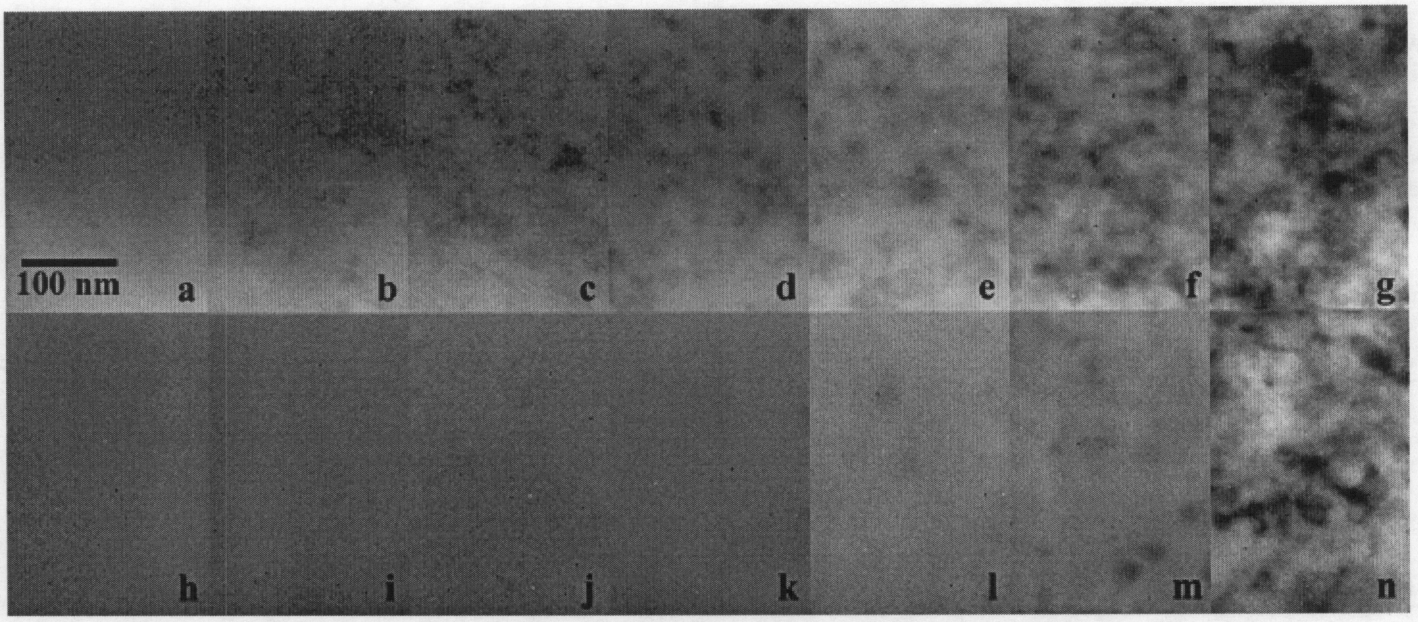

Figure 1. – TEM bright field images as viewed in cross-section of the $Be_{.84}B_{.16}$ sample in the (a) as-deposited condition, (b) at 200°C, (c) 250°C, (d) 275°C, (e) 300°C, (f) 325°C, and (g) 350°C as well as the $Be_{.79}B_{.21}$ (h) as-deposited, (i) at 200°C, (j) 250°C, (k) 275°C, (l) 300°C, (m) 325°C, and (n) 350°C.

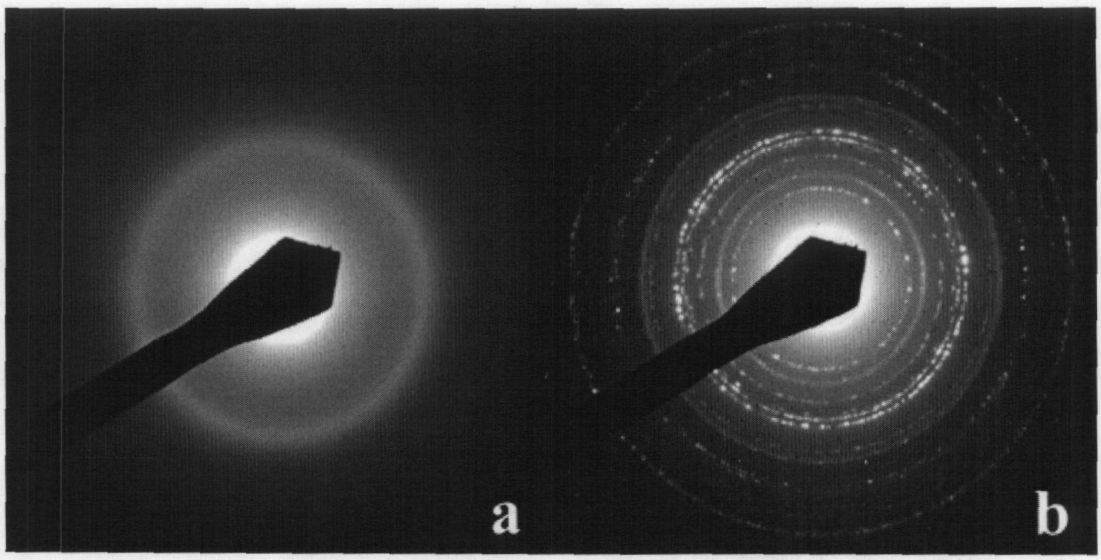

Figure 2. – SADPs taken from the cross-sectioned coatings of the $Be_{.79}B_{.21}$. sample (a) as-deposited, and (b) at 350°C.

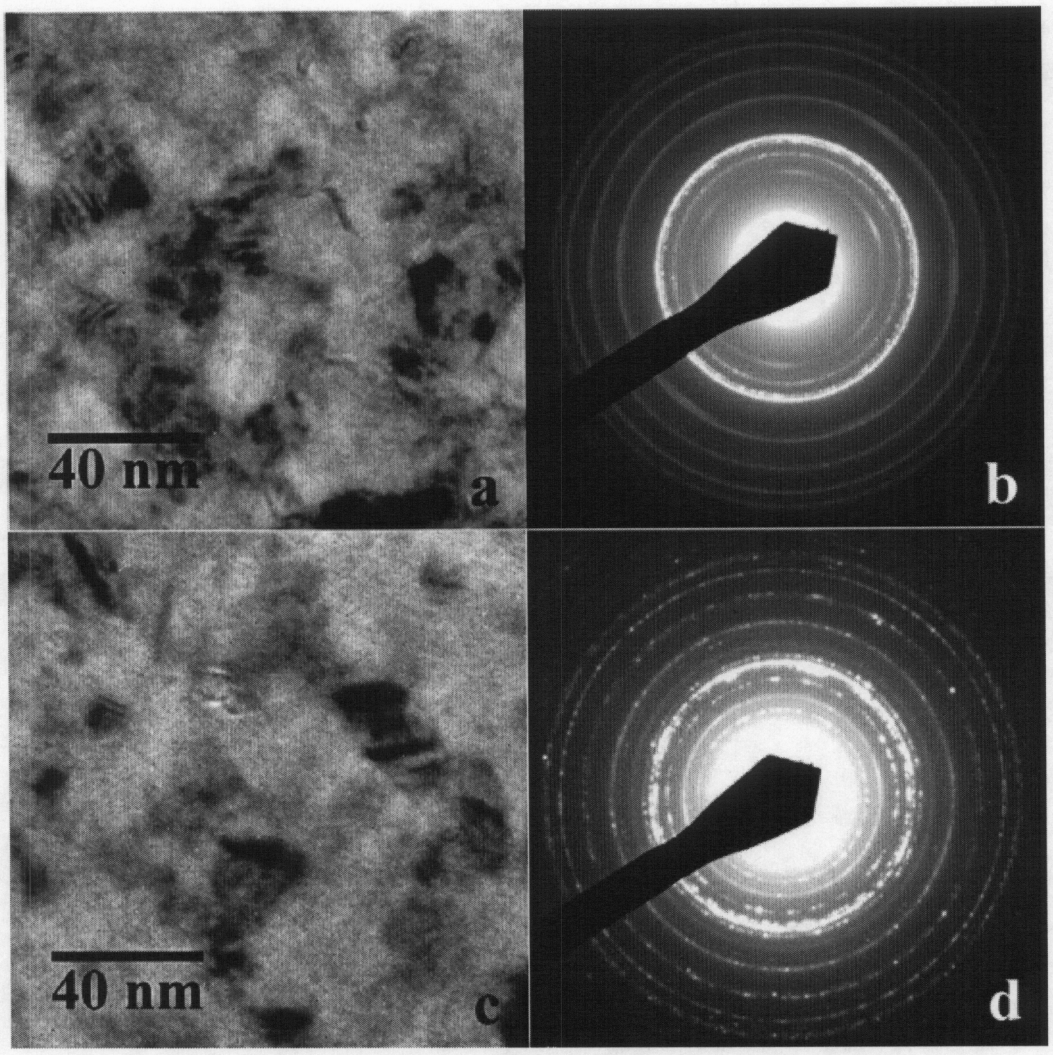

Figure 3. – TEM bright field images shown in plan view and SADPs, respectively, of the $Be_{.90}B_{.10}$ sample in the (a-b) as-deposited condition and (c-d) at 500°C.